Local structure of Y and Ho in calcite and its relevance to Y fractionation from Ho in partitioning between calcite and aqueous solution

Kazuya Tanaka, Yoshio Takahashi and Hiroshi Shimizu

Department of Earth and Planetary Systems Science
Graduate School of Science, Hiroshima University
Kagamiyama 1-3-1, Higashi-Hiroshima 739-8526, Japan

Revised version
November 8, 2007

* Corresponding Author: Kazuya Tanaka
E-mail address: tanaka@geol.sci.hiroshima-u.ac.jp
Phone: +81-82-424-7459
Fax: +81-82-424-0735

Abstract

Among rare earth elements (REEs), the behavior of Y and Ho in most igneous activities is very close due to the similarity in their ionic radii, while Y fractionates from Ho in marine systems. In this study, in order to elucidate Y-Ho fractionation observed in marine systems in terms of structural chemistry, we examined Ho L_{III}-edge and Y K-edge EXAFS study for two partitioning systems, namely, 1) calcite-aqueous solution (Y-Ho fractionation system) and 2) strong acid cation exchange resin-aqueous solution (non Y-Ho fractionation system). The results of the EXAFS analysis did not show significant differences in interatomic distances to the most neighboring O atoms between Ho and Y for all the samples. However, it was found that the first shell Ho-O and Y-O distances in the Y-Ho doped calcite were shorter than those in the aqua ion. In contrast, the first shell Ho-O and Y-O distances in the Y-Ho doped resin were similar to those in the aqua ion. Previous studies have suggested that lanthanide (Ln) is more covalent due to 4f orbital participation in bonding relative to Y. Spectroscopic studies on various Ln^{3+} complexes show that Racah parameters for 4f electron repulsion in Ln^{3+} ions decrease with an increase in covalency of bonding of Ln^{3+} ions with anionic ligands. Therefore, our EXAFS results suggest that Y-Ho fractionation in partitioning is possibly attributed to the difference of change in covalency associated with the ligand exchange between Y and Ho, which we have observed as differences in partition coefficients between calcite and aqueous solution.

Keywords: Y-Ho fractionation; EXAFS; local structure; covalency

1. Introduction

Rare earth elements (REEs) have received considerable attention because of their contribution to geochemical studies in various fields. In particular, the abundances of Y and Ho, one of lanthanides (Lns), are often compared as geochemical twins because the behavior of these trivalent elements in the natural environment is very similar due to their almost identical ionic radii (Shannon, 1976). Average upper continental materials such as NASC (North American shale composite) and PAAS (Post-Archean Australian average shale) have an Y/Ho weight ratio of 28, which is equal to the value of bulk earth composition derived from chondritic meteorite (Gromet et al., 1984; Taylor and McLennan, 1988; Anders and Grevesse, 1989). Mid-ocean-ridge and ocean-island basalts as well as spinel peridotite xenoliths also show the chondritic Y/Ho ratio (Jochum et al., 1986; Jochum et al., 1989), although Y/Ho ratios of highly evolved granitic rocks deviate from the chondritic value (Bau, 1996; Irber, 1999). This indicates that significant Y-Ho fractionation does not occur in most magmatic conditions except in highly evolved magmatic systems. On the other hand, Y fractionation from Ho in marine samples has been pointed out by many researchers. Present-day seawater, marine carbonates and phosphorites have Y/Ho ratios of 40-80 which are much higher than the chondritic value (Kawabe et al., 1991; Bau et al., 1995; Bau et al., 1996; Bau et al., 1997; Nozaki et al., 1997; Webb and Kamber, 2000; Kamber and Webb, 2001; Tanaka et al., 2003). In contrast, the Y/Ho ratios of deep-sea ferromanganese nodules and crusts are 17-25 (Bau et al., 1996; Ohta et al., 1999). Yttrium fractionation from Ho has been observed not only in natural samples but also in laboratory partitioning experiments. Partition coefficients between Fe oxyhydroxide and aqueous solution show that Ho is selectively coprecipitated with Fe oxyhydroxide relative to Y (Bau,

1999; Ohta and Kawabe, 2000). Ohta and Kawabe. (2001) reported the fractionation between Y and Ho in the adsorption onto δ-MnO_2 in aqueous solution. Similarly, Y-Ho fractionation was observed in the partitioning between calcite and aqueous solution (Tanaka et al., 2004; Tanaka and Kawabe, 2006).

The oxidation state of Y and Ho is trivalent in natural environments. The electron configuration of Ho(III) is $[Xe](4f)^{10}$, but Y(III), whose electron configuration is [Kr], does not have a 4f electron. Such difference in electron configuration may cause Y-Ho fractionation in certain systems, which cannot be explained simply by their ionic sizes due to their almost identical ionic radii (Shannon, 1976). Partition coefficients are related to thermodynamic equilibrium constants for partitioning reactions. In other words, a change in Gibbs free energy, ΔG, of the chemical species responsible for partitioning reactions is reflected in partition coefficients. This means that the difference of partition coefficients between Y and Ho (i.e., Y-Ho fractionation) is equivalent to that of the change in ΔG between Y and Ho. Hence, a change in the coordination structure of Y and Ho species must be observed as values of partition coefficients through thermodynamic parameters. X-ray absorption fine structure (XAFS) spectroscopy is useful for the direct observation of the local coordination structure and speciation of trace elements in both liquid and solid states. XAFS consists of two energy regions, namely, X-ray absorption near-edge structure (XANES) and extended X-ray absorption fine structure (EXAFS). In particular, EXAFS provides information on the local structure around a target atom, including the coordination number and interatomic distance. The aim of this study is to elucidate the Y-Ho fractionation in terms of the structural chemistry using EXAFS spectroscopy. In the present study, we employed EXAFS spectroscopy mainly to obtain the average

distances of the most neighboring atoms from Y and Ho. REE concentrations in natural samples are generally too low to obtain good EXAFS spectra. Therefore, we prepared a series of samples with relatively high REE concentrations related to Y-Ho fractionation. We selected two systems of REE partitioning between, 1) REE incorporated in calcite and REE solution and 2) REE adsorbed on a strong acid cation exchange resin and REE solution, in order to achieve our scientific goal. Yttrium-Ho fractionation occurs in the partitioning between calcite and aqueous solution (Tanaka et al., 2004; Tanaka and Kawabe, 2006), whereas Y does not fractionate from Ho between strong acid cation exchange resin and aqueous solution as shown below.

2. Material and Methods

2.1. Reference and synthetic materials

2.1.1. Reference materials

The EXAFS spectra of sesquioxide (Y_2O_3 and Ho_2O_3) and carbonate hydrate ($Y_2(CO_3)_3{\cdot}nH_2O$ and $Ho_2(CO_3)_3{\cdot}nH_2O$) were measured as solid reference materials together with the synthetic materials. The purity of all the reagents was more than 99.9%, which were diluted with boron nitride (BN) to the proper concentrations for EXAFS measurement in transmission mode. The concentrations of Y or Ho in the BN matrix were decided by the criterion that difference of absorbance between pre-edge and post-edge was 2.55, calculated based on Victoreen's equation and McMaster's table of mass absorption coefficients (McMaster, 1969).

Yttrium and Ho solutions as liquid reference materials were prepared through the dissolution of chloride hexahydrate ($YCl_3{\cdot}6H_2O$ and $HoCl_3{\cdot}6H_2O$) with Milli-Q water. The EXAFS measurements of Y^{3+} and Ho^{3+} aqua ions in aqueous solution, $Y^{3+}_{(aq)}$ and

$Ho^{3+}_{(aq)}$, were made using these solutions. The Y and Ho concentrations were adjusted to 0.13 and 0.055 mol/kg, respectively. According to the speciation calculation, about 90% of Y and Ho in each solution was aqua ion, whereas most of the remaining species was $REECl^{2+}_{(aq)}$. Despite the existence of $REECl^{2+}_{(aq)}$, our EXAFS data for the Y and Ho solutions were compatible with those for aqua ions previously reported as discussed below.

2.1.2. Synthetic materials

Calcite sample doped with Y and Ho was prepared using a simple co-precipitation method at room temperature. In calcite precipitation, Y and Ho were simultaneously co-precipitated. First, 0.20 M $NaHCO_3$ and Y-Ho spike solution (Y: 1.1 mmol/L, Ho: 0.6 mmol/L) were added to the $CaCl_2$-NaCl solution (Ca: 200 mmol/L, Na: 50 mmol/L), which was stirred with a magnetic stirrer chip. The initial Y and Ho concentrations in the solution were 22 μmol/L and 12 μmol/L, respectively. Then 0.20 M NaOH solution was further put into the solution to make calcite precipitates. When fine crystal started to form (pH ~ 8), stirring was stopped, and the prepared solution was filtered with a 0.45 μm filter immediately. The disadvantage of this approach is that the solution composition does not remain constant during the precipitation because the initial Ca and REE concentrations decrease due to calcite precipitation. This, however, is not a serious problem in the current study, as far as the mode of incorporation remains the same even if the solution composition changes. The solution was undersaturated with respect to $Y_2(CO_3)_3 \cdot nH_2O$ and $Ho_2(CO_3)_3 \cdot nH_2O$. The finely crystalline product after drying at 40°C was identified as calcite with XRD. X-ray diffraction did not show any reflections other than those of pure calcite.

Yttrium and Ho were simultaneously adsorbed onto a strong acid cation exchange resin (Bio-Rad AG50W-X8, 200-400 mesh) in the solution at pH = 1.5 under room temperature condition. The cation exchange resin is composed of a styrene divinylbenzene copolymer as matrix and sulfonic acid functional groups ($–SO_3^-$) attached to the copolymer. The proton exchange capacity of the cation resin is 2.1 meq/g. First, Y-Ho spike solution (Y: 1.1 mmol/L, Ho: 0.6 mmol/L) was added to Milli-Q water, in which the cation exchange resin was agitated with a magnetic stirrer chip. The initial Y and Ho concentrations in the solution were 220 μmol/L and 120 μmol/L, respectively. The pH of the Milli-Q water with the resin went below 1.5 due to the addition of the spike solution. A small amount of 0.2 M NaOH solution was then added to adjust the pH of the solution to 1.5. After filtration with a 0.45 μm filter, the resin was packed into a film bag without drying to prevent changes of the absorbed species.

Yttrium and Ho concentrations in the synthetic calcite, the Y-Ho doped resin and the corresponding solution samples were determined by ICP-MS (VG PQ-3). Yittrium and Ho were extracted from the Y-Ho doped resin using 6 M HCl before ICP-MS measurement. The analytical precision for Y and Ho was estimated to be better than 5%. The Y and Ho concentrations of the calcite sample were 3,200 mg/kg and 3,400 mg/kg, respectively, while those of the resin sample were 1,360 mg/kg and 1,380 mg/kg, respectively.

2.2. EXAFS spectroscopy

The Ho L_{III}-edge (8.074 keV) EXAFS spectra for all samples were collected at beamline 12C at Photon Factory, KEK (Tsukuba, Japan). A broad band synchrotron

radiation from storage ring operated at 2.5 GeV with a typical beam current of 450-300 mA was monochromatized with a Si (111) channel-cut double-crystal monochromator to obtain the incident X-ray beam. The spectra of Ho_2O_3, $Ho_2(CO_3)_3 \cdot nH_2O$ and $Ho^{3+}_{(aq)}$ as reference materials were collected by the transmission method. The fluorescence yield of the Y-Ho doped calcite and resin was monitored using a 19-element semiconductor Ge detector (SSD). In the fluorescence mode, each sample was placed at 45° to the X-ray beam. All the measurements were carried out at room temperature under ambient conditions.

The Y K-edge (17.037 keV) EXAFS spectra for all the samples were collected at beamline BL01B1 of SPring-8 (Hyogo, Japan). The SPring-8 storage ring was operated at 8.0 GeV electron energy with an electron current of 100 mA. A Si(111) double-crystal monochromator was used to obtain the incident X-ray beam. The spectra of the reference materials were collected in transmission mode. The calcite sample doped with Y and Ho was measured in fluorescence mode using a Lytle detector, whereas the Y-Ho doped resin sample was measured using SSD.

2.3. XAFS analysis

EXAFS data analysis was conducted using REX2000 ver.2.3 (Rigaku Co.) with parameters generated by FEFF7.02 (Zavinsky et al., 1995; Ankudinov and Rehr, 1997). The background absorption other than that of REE was subtracted using a linear function estimated from the pre-edge region for the spectra obtained by fluorescence mode. On the other hand, Victoreen function was used for the spectra obtained by transmission mode. After subtraction of background absorption and normalization, the smooth Ho L_{III}-edge and Y K-edge absorption of the free atom (μ_0) was removed using

a spline smoothing curve. The energy unit was transformed from keV to $Å^{-1}$ to produce the EXAFS function $\chi(k)$, where k ($Å^{-1}$) is the photoelectron wave vector given by $\sqrt{2m(E-E_0/\hbar^2)}$ (E is the energy of the incident X-ray; E_0 is the threshold energy for liberation of the photoelectron wave). In the present study, the E_0 value was initially determined from the maximum value in the derivative of $\chi(k)$ in the absorption region, which was finally optimized in the EXAFS simulation. The k^3-weighted $\chi(k)$ values were Fourier transformed from k (1/Å) space into R (Å) space to give a radial structural function (RSF). The theoretical EXAFS function was fitted to the back transformed k^3-weighted $\chi(k)$ functions using parameters including theoretical backscattering amplitudes and phase shifts generated by FEFF 7.02. The initial structural data by ATOMS (Ravel, 2001) were utilized to make FEFF parameters. During the simulation, it was found that the contribution of the second and further shells to the EXAFS function was minor in all samples, except for the sesquioxides of Ho_2O_3 and Y_2O_3. The EXAFS analysis gives the coordination number (CN), the interatomic distance (R) between the absorber and scatterer atoms, the Debye-Waller term (σ^2), and the energy offset (ΔE_0).

3. Results

3.1. Y-Ho fractionation between solid and solution

The apparent partition coefficients between synthetic calcite (or resin) and aqueous solution, K_d(REE), were calculated from the analytical results of ICP-MS. In calcite precipitation, about 95% of initially added Y and Ho were removed from the aqueous solution. On the other hand, 0.23% of initially added Y and Ho remained in the

aqueous solution after the adsorption experiment. Here, we define K_d(REE) simply as the concentration ratio of solid to solution (i.e. $K_d(REE) = [REE]_{solid}/[REE]_{solution}$) because our main interest is the relative partitioning behavior of Y to Ho. The calculated $K_d(Y)/K_d(Ho)$ values of calcite was 0.71, which indicates that Y fractionates from Ho during coprecipitaiton with calcite (Tanaka et al., 2004; Tanaka and Kawabe, 2006). In contrast, significant Y-Ho fractionation was not observed in the partitioning between strong acid cation exchange resin and aqueous solution ($K_d(Y)/K_d(Ho) = 0.94$).

3.2. XAFS spectra

Figure 1 shows the normalized XANES spectra for Ho and Y in aqueous solution, sesquioxides, carbonate hydrates, Y-Ho doped calcite and resin. The Ho L_{III}-edge spectra are similar to each other, although the white line peak of Ho_2O_3 is smaller and broader than those of the others (Fig. 1a). The Y K-edge spectra for Y_2O_3 and Y-Ho doped calcite show broad white line peaks relative to the Y solution, $Y_2(CO_3)_3 \cdot nH_2O$ and Y-Ho doped resin (Fig. 1b). In fact, splitting is observed around the fine structures of these white line peaks (Fig. 2). Such splitting for Y_2O_3 has been reported by previous studies (Li and Chen, 1993; Wang et al., 2002). The splitting for Y-Ho doped calcite may indicate that Y is incorporated into calcite crystals, but is not present as a mixture of Y incorporated in calcite and $Y_2(CO_3)_3 \cdot nH_2O$ because the Y-Ho doped calcite was synthesized in the solution which was undersaturated with respect to $Y_2(CO_3)_3 \cdot nH_2O$.

Figures 3 and 4 show the k^3-weighted EXAFS spectra $\chi(k)$ and RSFs. Previous studies reported the contribution of multi-electron excitations to EXAFS spectra in REE aqueous solution (e.g. Solera et al., 1995; D'Angelo et al., 2001). However, clear

evidence of the features in any of the EXAFS spectra attributable to multi-electron excitations was not observed in the spectra in Figs. 3a and 4a. The low-R peaks of Fourier transform (FT) magnitudes around ~1.8-1.9 Å (phase shift uncorrected) were attributed to the first shell of oxygen atoms (Figs. 3b and 4b). As noted above, no clear peaks at a higher R, which correspond to the second and further shells, were identified except for sesquioxides. The k^3-weighted EXAFS spectra $\chi(k)$ and the RSFs obtained by Fourier transforms from k^3-weighted $\chi(k)$ were simulated by the parameters generated by FEFF 7.02. The starting model used for the FEFF calculation of Y-Ho doped calcite sample was based on the calcite structure assuming that REE substitutes for the Ca site (Elzinga et al., 2002). The analytical results of best-fit parameters are shown in Table 1.

3.3. Interatomic distances estimated from EXAFS analysis

The hydration (coordination) number of REE and interatomic distances between REE and oxygen of water molecule in aqueous solution have been well studied (Habenschuss and Spedding, 1979a; Habenschuss and Spedding, 1979b; Habenschuss and Spedding, 1980; Yamaguchi et al., 1988; Díaz-Moreno et al., 2000). The hydration number of heavy REE and Y is 8, whereas that of light REE is 9. The coordination number was therefore fixed to 8 in the simulation of $Ho_{(aq)}$ and $Y_{(aq)}$. The fitting results gave 2.351 and 2.354 Å for the first shell REE-O distances of aqua Ho and Y ions, respectively (Table 1). Yamaguchi et al. (1988) reported Dy-OH_2 (2.37 Å) and Er-OH_2 (2.34 Å) distances in aqueous REE perchlorate solutions using EXAFS. From the interpolation of these distances, Ho-OH_2 bond length was estimated to be 2.35-2.36 Å. Díaz-Moreno et al. (2000) also reported the distance (2.35 Å) between Y and H_2O

molecule using EXAFS. Our results are therefore compatible with those of the previous studies.

The Ho-O distance (2.351 Å) in $Ho_2(CO_3)_3 \cdot nH_2O$ is identical to the Y-O distance (2.360 Å) in $Y_2(CO_3)_3 \cdot nH_2O$ within errors of simulation for bond length (Table 1). The Y atom in tengerite-(Y), $Y_2(CO_3)_3 \cdot nH_2O$ (n=2-3), is coordinated by eight O atoms of carbonate ions and one of H_2O, with Y-O distances ranging from 2.34 to 2.53 Å (Miyawaki et al., 1993). Consequently, the calculated values of Ho-O and Y-O distances in the Y-Ho carbonate hydrates indicated an average of nine different distances.

The REE sesquioxides can be hexagonal (A-type), monoclinic (B-type) or cubic (C-type). The structures of the sesquioxides follow the trend A→B→C as the ionic radius decreases. The C-type REE sesquioxides have the mineral bixbyite (Mn_2O_3) structure with two distinct REE sites, both having sixfold coordination. The average REE-O distances in the different sites of C-type sesquioxides are approximately the same (Maslen et al., 1996). Moreover, the average interatomic distance between Ho and O (2.283 Å) is almost equal to that between Y and O (2.282 Å) (Maslen et al., 1996). On the other hand, the first-shell Ho-O and Y-O distances determined in this study were 2.279 and 2.270 Å, respectively (Table 1). Our estimation of interatomic distances between REE and O in sesquioxides was in good agreement with those estimated by Maslen et al. (1996).

The first shell Ho-O and Y-O distances in Y-Ho doped calcite (2.310 and 2.311 Å, respectively) were 0.05 Å shorter than the Ca-O distance in ideal calcite (2.36 Å) (Table 1). Elzinga et al. (2002) measured the EXAFS spectra for synthetic calcite samples doped with some REEs (Nd, Sm, Dy and Yb). From their EXAFS analysis, they

concluded that REEs were substituted for Ca in calcite structure. The interatomic distance of Dy-O in REE doped calcite was estimated at 2.30 Å by Elzinga et al. (2002). Taking into account ± 0.02 errors for the distances estimated by the simulation, the Ho-O distance of 2.311 Å in this study was compatible with the Dy-O distance by Elzinga et al. (2002). In addition, it was unlikely that Ho or Y carbonate precipitation occurred simultaneously during the coprecipitation of calcite with Ho and Y because the Ho-O and Y-O distances in the calcite sample were shorter than those in the REE-carbonate hydrates (Table 1). The Ho-O and Y-O distances determined in the present study indicated that Ho and Y were substituted for Ca in calcite as Elzinga et al. (2002) concluded. The observed splitting of a white line peak in the Y spectrum of the calcite sample, which was not observed in the spectrum of $Y_2(CO_3)_3 \cdot nH_2O$, may indicate Y substitution for Ca in calcite (Fig. 2). Despite the fairly rapid precipitation rate of this study, the result obtained here is consistent with that of Elzinga et al. (2002), in which calcite was precipitated under steady state with constant pH over a few weeks. Hence, it is unlikely that the precipitation rate of calcite has an effect on REE-O distances in this time scale. The coordination numbers of the first shell oxygen for Ho and Y in the synthetic calcite sample were estimated to be 5.8 and 6.1, respectively (Table 1). These values are consistent with the fact that Ca is sixfold in the ideal calcite structure, although the coordination number determined by EXAFS analysis is generally accompanied by ± 20% errors.

The bond lengths of Ho-O and Y-O in the resin sample were calculated as 2.360 and 2.349 Å, respectively, with the coordination number of 8.2 (Table 1). The interatomic distances and coordination numbers for the resin sample were similar to those for aqua ions. The adsorbed cations in strong acid cation exchange resin form outer sphere

complexes with sulfonic acid functional groups attached to a styrene divinylbenzene copolymer lattice (Takahashi et al., 1997). Therefore, the similarity of the bond lengths and coordination numbers between the resin sample and aqua ion was reasonable.

4. Discussion

4.1. Y-Ho partitioning between calcite and aqueous solution

The REE incorporation mechanism into the calcite structure has been discussed by several researchers. For instance, Zhong and Mucci (1995) suggested that Na^+ compensates for excess charge of REE substitution for the Ca site, whereas such charge balanced substitution was abandoned by Lakshtanov and Stipp (2004). In any case, if the incorporation mechanism of Ho is different from that of Y, Y-Ho fractionation is expected to occur. However, the incorporation mechanisms of Ho and Y are probably the same because the first shell distances and coordination numbers of Ho-O and Y-O are very similar (Table 1). Therefore, other possibilities should be examined to explain Y-Ho fractionation as discussed in the following section.

The REE carbonate complexes of $REECO_3^+{}_{(aq)}$ and $REE(CO_3)_2^-{}_{(aq)}$ are dominant in an aqueous solution at a high concentration of dissolved carbonate ion (e.g., seawater) due to their large complexation constants (Liu and Byrne, 1998; Ohta and Kawabe, 2000). According to speciation calculation, the dominant REE species in our experimental solution used for calcite precipitation were carbonate complexes because we synthesized the calcite sample using aqueous solution with relatively high pH and total carbonate concentration. In particular, $REE(CO_3)_2^-{}_{(aq)}$ occupies 80 – 90% of the total REE species for heavy REEs and Y. This means that the K_d(REE) determined in this

study corresponds to the partition coefficient between REE species in calcite and $REE(CO_3)_2^-{}_{(aq)}$ (or $REECO_3^+{}_{(aq)}$). The REE-O distances in Y-Ho doped calcite and carbonate complexes should be compared in order to discuss the relationship between Y-Ho fractionation and interatomic distances. Unfortunately, it is difficult to obtain EXAFS spectra for the dissolved complexes of REE carbonate, because REE precipitation occurs in a solution with high REE and carbonate concentrations. It is, however, possible to discuss the Y-Ho fractionation between Y-Ho in calcite and free Y-Ho in aqueous solution, when K_d(REE) is corrected to the partition coefficient between REE species in calcite and aqua ions using REE carbonate complexation constants. Our $K_d(Y)/K_d(Ho)$ ratio between calcite and aqueous solution was corrected from 0.71 to 0.47 according to Tanaka et al. (2004) and Tanaka and Kawabe (2006). The decrease in $K_d(Y)/K_d(Ho)$ due to correction indicates that Y-Ho fractionation also occurs during carbonate complexation, which is observed as carbonate complexation constants (Liu and Byrne, 1998; Ohta and Kawabe, 2000).

4.2. Relationship between interatomic distance and Y-Ho fractionation

Errors in the fitted parameters are estimated to be generally ± 0.02 Å for the first-shell distance. Significant differences between Y and Ho in the first-shell REE-O distances for each sample were not observed (Table 1). It should be noted, however, that Ho-O and Y-O distances in calcite were shorter than those in aqua ion, whereas Ho-O and Y-O distances in the resin were similar to those in aqua ions. Bond lengths are related to the covalency of respective bondings, which is referred to as covalent shortening (Shannon, 1976). The first shell REE-O distances in REE-doped calcite reported by Elzinga et al. (2002) are also shorter than the corresponding REE-OH_2

distances of aqua ions reported by Yamaguchi et al. (1988). In other words, this suggests that REE-O bonds in calcite are more covalent than those of aqua ions and REE adsorbed onto resin. Compared with Y, lanthanide is more covalent due to 4f orbital participation in bonding (Mioduski, 1993). Spectroscopic studies on various Ln^{3+} complexes show that the Racah parameters for 4f electron repulsion in Ln^{3+} ions decrease with the increasing covalency of bonding of Ln^{3+} ions with anionic ligands. This is known as the nephelauxetic series (Jørgensen, 1979; Caro et al., 1981). Y-Ho fractionation in partitioning is possibly attributed to the difference of change in the covalency of bonding associated with the ligand exchange between Y and Ho. This is supported by the fact that in the non Y-Ho fractionation system (resin-solution), the Ho-O and Y-O distances and coordination numbers in the resin were similar to those in aqua ions, which is attributed to the similarity of coordination structure between aqua REE^{3+} ion and REE^{3+} adsorbed onto strong acid cation exchange resin (Takahashi et al., 1997).

Significant differences in interatomic distances from the most neighboring O atoms between Ho and Y were not observed for all the samples including the reference and synthetic materials (Table 1). As noted above, the bonding nature of Ho and Y, which is reflected in partition coefficients through thermodynamic parameters, is an important clue to understanding Y-Ho fractionation during various partitioning processes. The relationship between Y-Ho fractionation and the systematic change of coordination structure can be observed in a sequence of $REE^{3+}_{(aq)}$, $REECO_3^{+}_{(aq)}$, $REE(CO_3)_2^{-}_{(aq)}$ and REE incorporated into calcite. The water molecules in the first coordination spheres of REE^{3+} ions are successively replaced by CO_3^{2-} among these REE species. These REE species have systematically different H_2O/CO_3^{2-} ratios in the first coordination spheres

of REE^{3+} ions. REE carbonate complexation constants show that Y-Ho fractionation occurs during reactions of $REE^{3+}_{(aq)} + CO_3^{2-}_{(aq)} = REECO_3^{+}_{(aq)}$ and $REECO_3^{+}_{(aq)} + CO_3^{2-}_{(aq)} = REE(CO_3)_2^{-}_{(aq)}$ (Liu and Byrne, 1998; Ohta and Kawabe, 2000). Similarly, the results of this study and those of Tanaka and Kawabe (2006) indicate that Y fractionates from Ho during the incorporation of $REE(CO_3)_2^{-}_{(aq)}$ (or $REECO_3^{+}_{(aq)}$) into calcite. It is expected that significant Y-Ho fractionation occurs especially when a change in the coordination structure of Y and Ho before and after ligand exchange is large during partitioning reaction. In this sense, the results of this study would help in understanding geochemical processes that cause Y-Ho fractionation.

5. Conclusions

We have measured Ho L_{III}-edge and Y K-edge EXAFS spectra for reference (aqua ion, sesquioxide and carbonate hydrate) and synthetic (Y-Ho doped calcite and strong acid cation exchange resin) materials. The first shell Ho-O distance was very similar to the first shell Y-O distance for each of these materials. In the Y-Ho fractionation system, the first shell Ho-O and Y-O distances in the Y-Ho doped calcite were shorter than those in the aqua ion. In contrast, in the non Y-Ho fractionation system, the first shell Ho-O and Y-O distances in the Y-Ho doped resin were similar to those in aqua ions. These EXAFS results of the interatomic distances suggest that REE-O bonds in calcite are more covalent than those of aqua ions and REE adsorbed onto the resin. This indicates that Y-Ho fractionation in partitioning is possibly attributed to the difference of change in the covalency of bonding associated with ligand exchange between Y and Ho.

Acknowledgements

This work was supported by a grant from the Japan Society for the Promotion of Science (JSPS) Research Fellowships for Young Scientists. It has been performed with the approval of SPring-8 (Proposal No. 2006A1533, 2006A1596 and 2006B1099) and Photon Factory, KEK (Proposal No. 2004G334 and 2006G336). Constructive comments from M. Bau and an anonymous reviewer improved the manuscript. We likewise thank S. Goldstein for his editorial management.

References

Anders, E., Grevesse, N., 1989. Abundances of the elements: Meteoritic and solar. Geochim. Cosmochim. Acta 53, 197-214.

Ankudinov A. L., Rehr J. J., 1997. Relativistic calculations of spin-dependent x-ray absorption spectra. Phys. Rev. B56, 1712-1716.

Bau, M., 1996. Controls on the fractionation of isovalent trace elements in magmatic and aqueous systems: evidence from Y/Ho, Zr/Hf, and lanthanide tetrad effect. Contrib. Mineral. Petrol. 123, 323-333.

Bau, M., 1999. Scavenging of dissolved yttrium and rare earths by precipitating iron oxyhydroxide: Experimental evidence for Ce oxidation, Y-Ho fractionation, and lanthanide tetrad effect. Geochim. Cosmochim. Acta 63, 67-77.

Bau, M., Dulski, P., Möller P., 1995. Yttrium and Holmium in South Pacific Seawater: Vertical Distribution and Possible Fractionation Mechanisms. Chem. Erde 55, 1-15.

Bau, M., Koschinsky, A., Dulski, P., Hein, J. R., 1996. Comparison of the partitioning behaviours of yttrium, rare earth elements, and titanium between hydrogenetic marine ferromanganese crusts and seawater. Geochim. Cosmochim. Acta 60, 1709-1725.

Bau, M., Möller, P., Dulski, P., 1997. Yttrium and lanthanides in eastern Mediterranean seawater and their fractionation during redox-cycling. Mar. Chem. 56, 123-131.

Caro, P., Deroouet, J., Beaury, L., Teste de Sagey, G., Chaminade, J. P., Aride, J., Pouchard, M. J., 1981. Interpretation of the optical absorption spectrum and paramagnetic susceptibility of neodymium trifluoride. J. Chem. Phys. 74, 2698-2704.

D'Angelo, P., Pavel, N. V., Borowski, M., 2001. K- and L-edge XAFS determination of the local structure of aqueous Nd(III) and Eu(III). J. Synchrotron Rad. 8, 666-668.

Díaz-Moreno, S., Muñoz-Páez, A., Chaboy, J., 2000. X-ray absorption spectroscopy (XAS) study of the hydration structure of yttrium(III) cations in liquid and glassy states: Eight or nine-fold coordination? J. Phys. Chem. A 104, 1278-1286.

Elzinga, E. J., Reeder, R. J., Withers, S. H., Peale, R. E., Mason, R. A., Beck, K. M., Hess, W. P., 2002. EXAFS study of rare-earth element coordination in calcite. Geochim. Cosmochim. Acta 66, 2875-2885.

Gromet, L. P., Dymek, R. F., Haskin, L. A., Korotev, R. L., 1984. The "North American shale composite": its compilation, major and trace element characteristics. Geochim. Cosmochim. Acta 48, 2469-3482.

Habenschuss, A., Spedding, F. H., 1979a. The coordination (hydration) of rare earth ions in aqueous chloride solutions from x-ray diffraction. I. $TbCl_3$, $DyCl_3$, $ErCl_3$, $TmCl_3$, and $LuCl_3$. J. Chem. Phys. 70, 2797-2806.

Habenschuss, A., Spedding, F. H., 1979b. The coordination (hydration) of rare earth ions in aqueous chloride solutions from x-ray diffraction. II. $LaCl_3$, $PrCl_3$, and $NdCl_3$. J. Chem. Phys. 70, 3758-3763.

Habenschuss, A., Spedding, F. H., 1980. The coordination (hydration) of rare earth ions in aqueous chloride solutions from x-ray diffraction. III. $SmCl_3$, $EuCl_3$, and series behavior. J. Chem. Phys. 73, 442-450.

Irber, W., 1999. The lanthanide tetrad effect and its correlation with K/Rb, Eu/Eu*, Sr/Eu, Y/Ho, and Zr/Hf of evolving peraluminous granite suites. Geochim. Cosmochim. Acta 63, 489-508.

Jochum, K. P., Seufert, H. M., Spettel, B., Palme, H., 1986. The solar-system abundances of Nb, Ta, and Y, and the relative abundances of refractory lithophile elements in differentiated planetary bodies. Geochim. Cosmochim. Acta 50, 1173-1183.

Jochum, K. P., McDonough, W. F., Palme, H., Spettel, B., 1989. Compositional constraints on the continental lithospheric mantle from trace elements in spinel peridotite xenoliths. Nature 340, 548-550.

Jørgensen, C. K., 1979. Theoretical chemistry of rare earths. In: Gschneidner, Jr. K. A., Eyring, L., (Eds.), Handbook on the Physics and Chemistry of Rare Earths. North-Holland, vol. 3, 111-169.

Kamber, B. S., Webb, G. E., 2001. The geochemistry of late Archaean microbial carbonate: Implications for ocean chemistry and continental erosion history. Geochim. Cosmochim. Acta 65, 2509-2525.

Kawabe, I., Kitahara, Y., Naito, K., 1991. Non-chondritic yttrium/holmium ratio and lanthanide tetrad effect observed in Pre-Cenozoic limestones. Geochem. J. 25, 31-41.

Lakshtanov, L. Z., Stipp, S. L. S., 2004. Experimental study of europium (III) coprecipitation with calcite. Geochim. Cosmochim. Acta 68, 819-827.

Li, P., Chen, I-W., 1993. X-ray-absorption studies of zirconia polymorphs. II. Effect of Y_2O_3 dopant on ZrO_2 structure. Phys. Rev. B 48, 10074-10081

Liu, X., Byrne, R. H., 1998. Comprehensive investigation of yttrium and rare earth element complexation by carbonate ions using ICP-Mass spectrometry. J. Sol. Chem. 27, 803-815.

Maslen, E. N., Streltsov, V. A., Ishizawa, N., 1996. A synchrotron X-ray study of the

electron density in c-type rare earth oxides. Acta Crystallogr. B52, 414-422.

McMaster, W. H., Kerr Del Grande, N., Mallet, J. H. and Hubell, J. H., 1969. Compilation of X-ray Cross Section. National Technical Information Service http://ixs.csrri.iit.edu/database/programs/index.html.

Mioduski, T., 1993. Covalency of Sc(III), Y(III), Ln(III) and An(III) as manifested in the enthalpies of solution of anhydrous rare earth halides. J. Radioanal. Nucl. Chem. 176, 371-382.

Miyawaki, R., Kuriyama, J., Nakai, I., 1993. The redefinition of tengerite-(Y), $Y_2(CO_3)_3 \cdot 2\text{-}3H_2O$, and its crystal structure. Am. Mineral. 78, 425-432.

Nozaki, Y., Zhang, J., Amakawa, H., 1997. The fractionation between Y and Ho in the marine environment. Earth Planet. Sci. Lett. 148, 329-340.

Ohta, A., Kawabe, I., 2000. Rare earth element partitioning between Fe oxyhydroxide precipitates and aqueous NaCl solutions doped with $NaHCO_3$: Determinations of rare earth element complexation constants with carbonate ions. Geochem. J. 34, 439-454.

Ohta, A., Kawabe, I., 2001. REE(III) adsorption onto Mn dioxide (δ-MnO_2) and Fe oxyhydroxide: Ce(III) oxidation by δ-MnO_2. Geochim. Cosmochim. Acta 65, 695-703.

Ohta, A., Ishii, S., Sakakibara, M., Mizuno, A., Kawabe, I., 1999. Systematic correlation of the Ce anomaly with the Co/(Ni+Cu) ratio and Y fractionation from Ho in distinct types of Pacific deep-sea nodules. Geochem. J. 33, 399-417.

Ravel, B., 2001. ATOMS: crystallography for the X-ray absorption spectroscopy. J. Synchrotron Radiat. 8, 314-316.

Shannon, R. D., 1976. Revised effective ionic radii and systematic studies of

interatomic distances in halides and chalcogenides. Acta Crystallogr. A32, 751-767.

Solera, J. A., García, J., Proietti, M. G., 1995. Multielectron excitations at the L edges in rare-earth ionic aqueous solutions. Phys. Rev. B51, 2678-2686.

Takahashi, Y., Kimura, T., Kato, Y., Minai, Y., Tominaga, T., 1997. Hydration structure of Eu^{III} on aqueous ion-exchange resins using laser-induced fluorescence spectroscopy. Chem. Commun. 223-224.

Tanaka, K., Kawabe, I., 2006. REE abundances in ancient seawater inferred from marine limestone and experimental REE partition coefficients between calcite and aqueous solution. Geochem. J. 40, 425-435.

Tanaka, K., Miura, N., Asahara, Y., Kawabe I., 2003. Rare earth element and strontium isotopic study of seamount-type limestones in Mesozoic accretionary complex of Southern Chichibu Terrane, central Japan: Implication for incorporation process of seawater REE into limestones. Geochem. J. 37, 163-180.

Tanaka, K., Ohta, A., Kawabe, I., 2004. Experimental REE partitioning between calcite and aqueous solution at 25°C and 1 atm: Constraints on the incorporation of seawater REE into seamount-type limestones. Geochem. J. 38, 19-32.

Taylor, S. R., McLennan, S. M., 1988. The significance of the rare earths in geochemistry and cosmochemistry. In: Gschneidner, Jr. K. A., Eyring, L. (Eds.), Handbook on the Physics and Chemistry of Rare Earths. Elsevier, Amsterdam, vol. 11, 485-578.

Wang, C. M., Cargill, G. S. III, Chan, H. M., Harmer, M. P., 2002. X-ray absorption near-edge structure of grain-boundary-segregated Y and Zr in creep-resistant alumina. J. Am. Ceram. Soc. 85, 2492-2498.

Webb, G. E., Kamber, B. S., 2000. Rare earth elements in Holocene reefal microbialites: A new shallow seawater proxy. *Geochim. Cosmochim. Acta* **64**, 1557-1565.

Yamaguchi, T., Nomura, M., Wakita, H., Ohtaki H., 1988. An extended x-ray absorption fine structure study of aqueous rare earth perchlorate solutions in liquid and glassy states. J. Chem. Phys. 89, 5153-5159.

Zavinsky, S. I., Rehr, J. J., Ankudinov, A., Albers, R. C., Eller, M. J., 1995. Multiple Scattering Calculations of X-ray Absorption Spectra. Phys. Rev. B52, 2995-3009.

Zhong, S., Mucci, A., 1995. Partitioning of rare earth elements (REEs) between calcite and seawater solutions at 25°C and 1 atm, and high dissolved REE concentrations. Geochim. Cosmochim. Acta 59, 443-453.

Figure captions

Fig. 1. The near-edge regions of the normalized (a) Ho L_{III}-edge and (b) Y K-edge absorption spectra of the reference and synthetic materials.

Fig. 2. Fine structures of white line peaks observed in the K-edge absorption spectra for Y_2O_3 and Y-Ho doped calcite.

Fig. 3. The EXAFS results for Ho in the reference and synthetic materials including (a) k^3-weighted $\chi(k)$ and (b) RSF (not phase shift corrected). Fitting results are shown as dashed lines.

Fig. 4. EXAFS results for Y in the reference and synthetic materials including (a) k^3-weighted $\chi(k)$ and (b) RSF (not phase shift corrected). Fitting results are shown as dashed lines.

Table 1. Best-fit parameters for EXAFS analyses obtained by the simulation using parameters generated by FEFF 7.02.[a,b]

Sample	Analyzed shells	Shell	CN	R (Å)	ΔE_0 (eV)	σ^2 (x 10^3)
Ho solution	1 shell	Ho-O	8.0[c]	2.351 ± 0.006	-3.1 ± 0.7	7.4 ± 0.1
Ho in calcite	1 shell	Ho-O	5.8 ± 0.5	2.311 ± 0.006	-3.4 ± 0.8	4.9 ± 0.1
Ho-exchanged resin	1 shell	Ho-O	8.2 ± 0.7	2.360 ± 0.006	-2.0 ± 0.7	5.8 ± 0.2
$Ho_2(CO_3)_3 \cdot nH_2O$	1 shell	Ho-O	9.0[c]	2.351 ± 0.006	-2.9 ± 0.8	5.6 ± 0.2
Ho_2O_3	4 shells	Ho-O	6.0[c]	2.279 ± 0.007	2.5 ± 1.0	5.8 ± 0.1
		Ho-Ho	6.0[c]	3.538 ± 0.027		3.2
		Ho-O	12.0[c]	3.727 ± 0.023		3.6
		Ho-Ho	6.0[c]	4.016		4.4
Y solution	1 shell	Y-O	8.0[c]	2.354 ± 0.005	-7.9 ± 0.9	5.8 ± 0.02
Y in calcite	1 shell	Y-O	6.1 ± 0.6	2.310 ± 0.007	-7.3 ± 1.1	6.2 ± 0.1
Y-exchanged resin	1 shell	Y-O	8.2 ± 0.7	2.349 ± 0.007	-4.5 ± 0.9	5.6 ± 0.2
$Y_2(CO_3)_3 \cdot nH_2O$	1 shell	Y-O	9.0[c]	2.360 ± 0.009	-6.1 ± 1.2	8.5 ± 0.2
Y_2O_3	4 shells	Y-O	6.0[c]	2.270 ± 0.006	-6.4 ± 1.1	5.0 ± 0.1
		Y-Y	6.0[c]	3.528 ± 0.011		3.1
		Y-O	12.0[c]	3.740		3.6
		Y-Y	6.0[c]	4.006		5.2

(a) CN: coordination number; R: interatomic distance; ΔE_0: threshold E_0 shift; σ: Debye-Waller term.

(b) Least squares precision is given to each value.

(c) Fixed in the simulation.

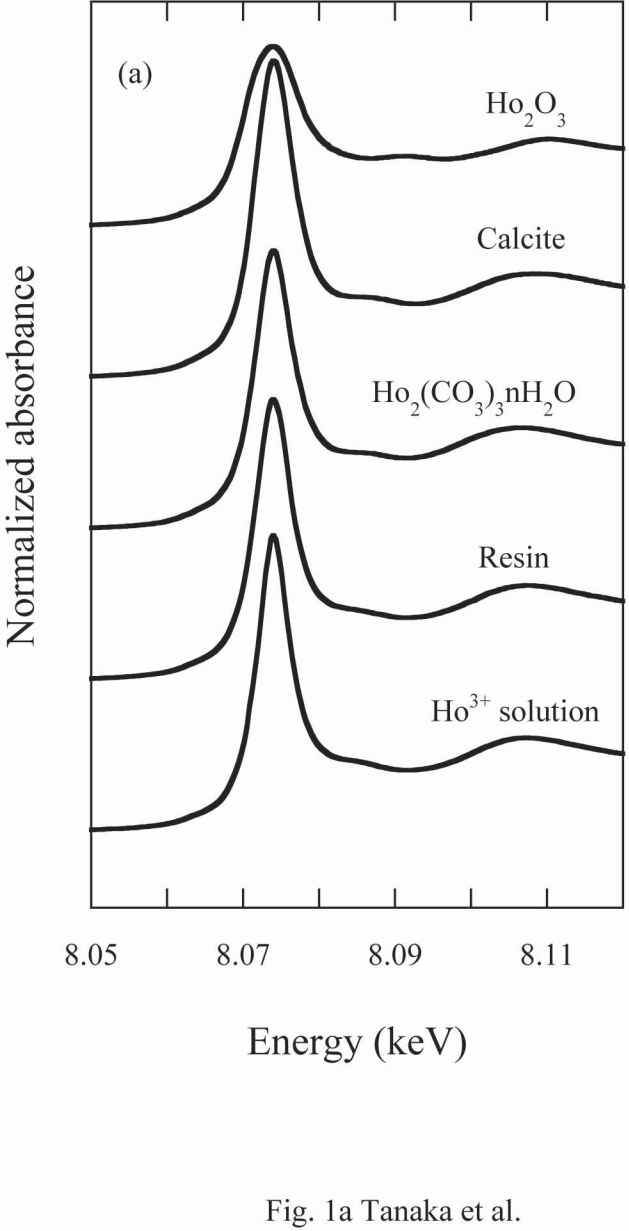

Fig. 1a Tanaka et al.

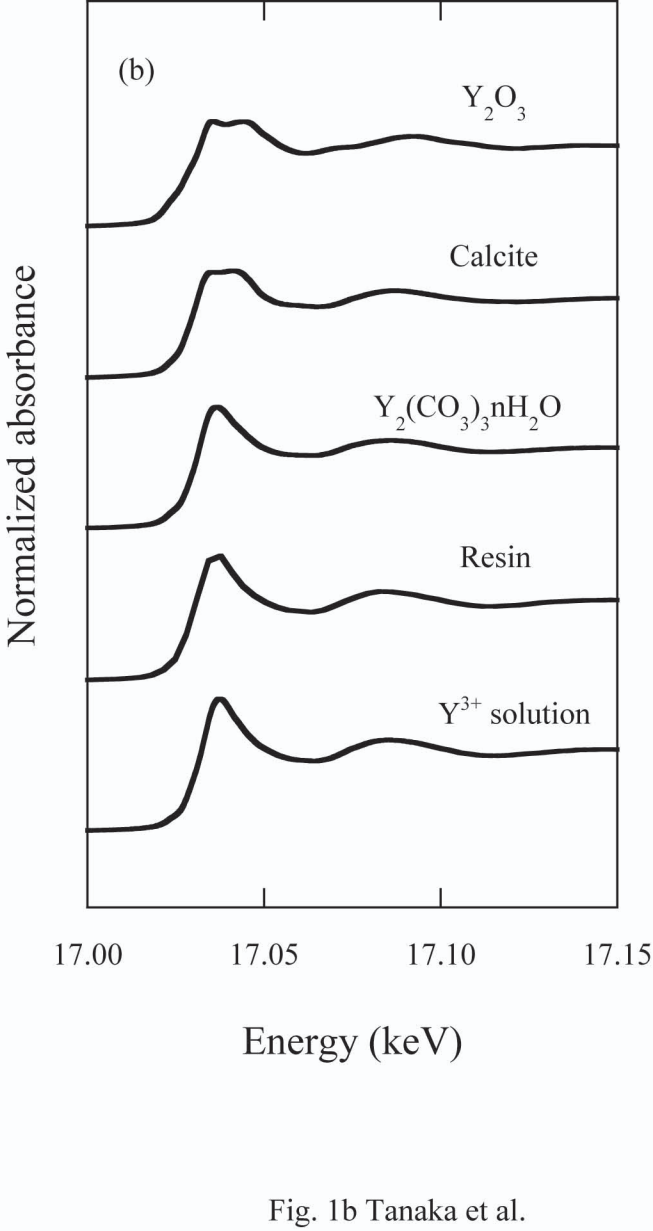

Fig. 1b Tanaka et al.

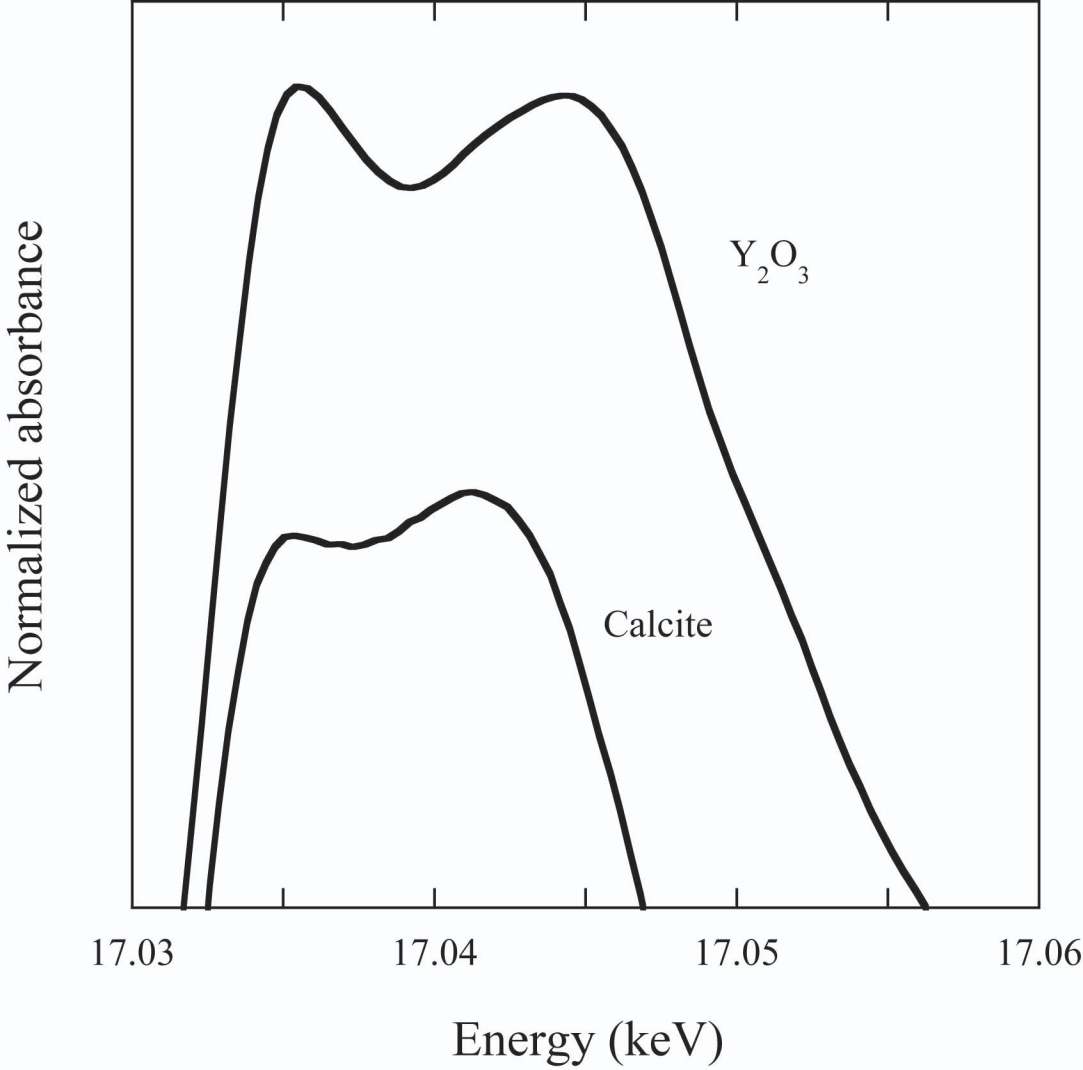

Fig. 2 Tanaka et al.

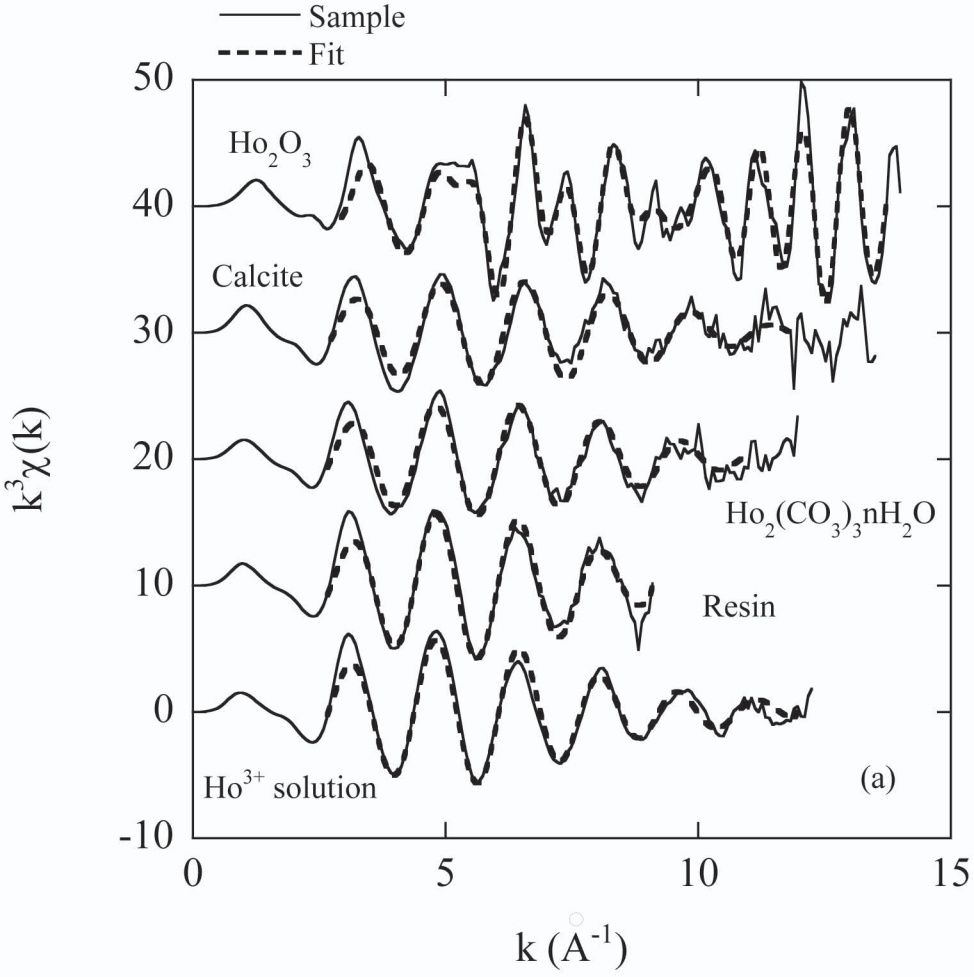

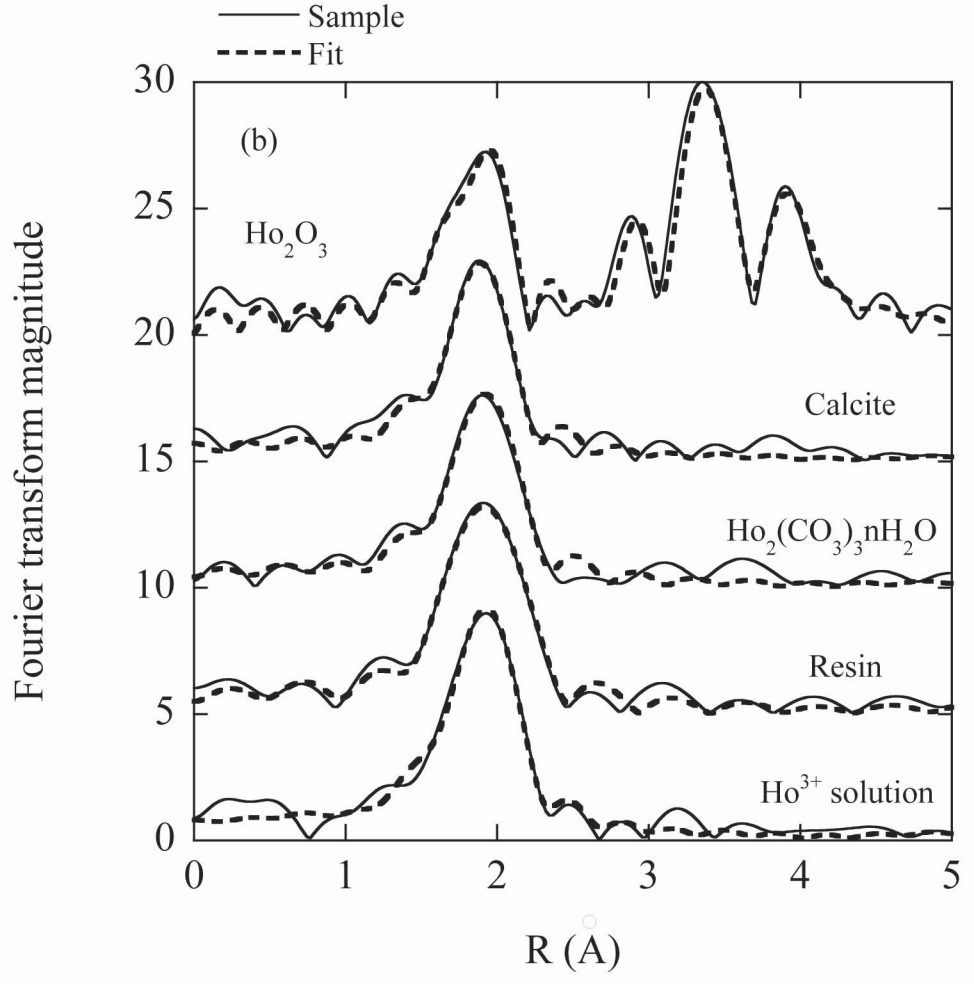

Fig. 3 Tanaka et al.

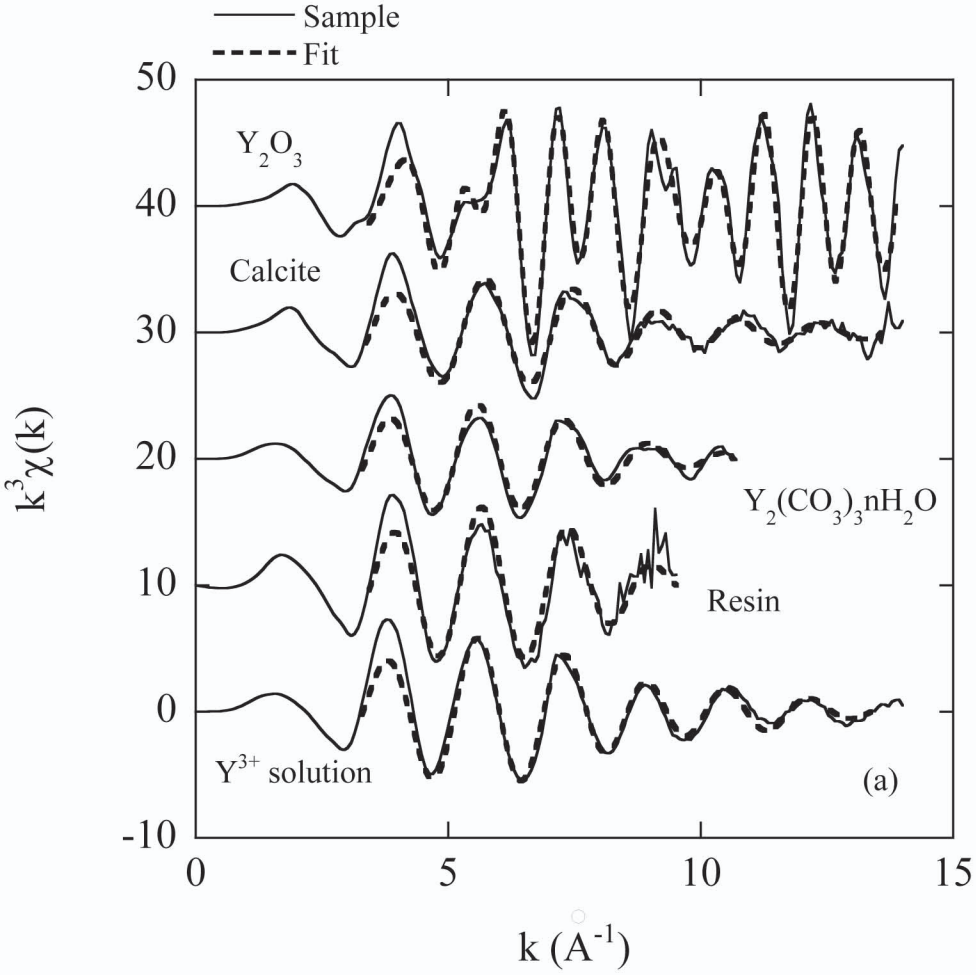

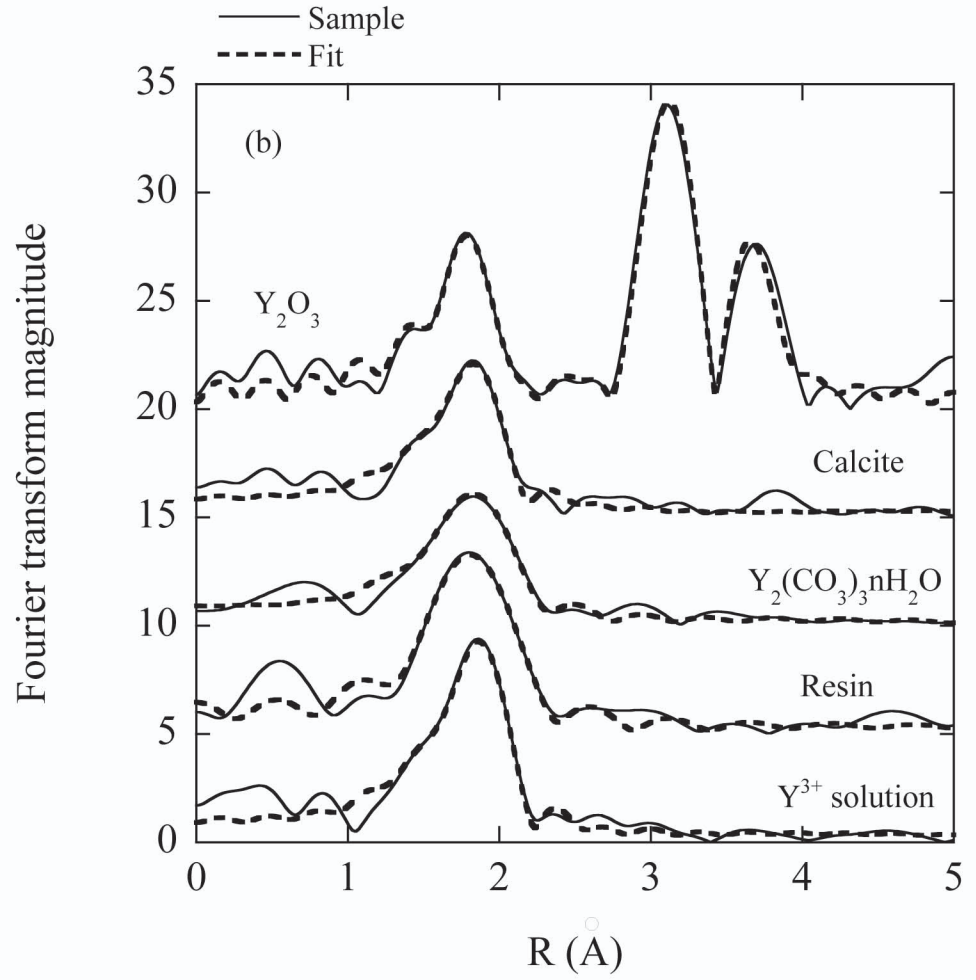

Fig. 4 Tanaka et al.